
EvenNet: Ignoring Odd-Hop Neighbors Improves Robustness of Graph Neural Networks

Runlin Lei

veritas@163.sufe.edu.cn

Zhewei Wei

zhewei@ruc.edu.cn

Zhen Wang

joneswong.ml@gmail.com

Yaliang Li

yaliang.li@gmail.com

Bolin Ding

atlas.ding@gmail.com

Abstract

Graph Neural Networks (GNNs) have received extensive research attention for their promising performance in graph machine learning. Despite their extraordinary predictive accuracy, existing approaches, such as GCN and GPRGNN, are not robust in the face of homophily changes on test graphs, rendering these models vulnerable to graph structural attacks and with limited capacity in generalizing to graphs of varied homophily levels. Although many methods have been proposed to improve the robustness of GNN models, the majority of these techniques are restricted to the spatial domain and employ complicated defense mechanisms, such as learning new graph structures or calculating edge attentions. In this paper, we study the problem of designing simple and robust GNN models in the spectral domain. We propose EvenNet, a spectral GNN corresponding to an even-polynomial graph filter. Based on our theoretical analysis in both spatial and spectral domains, we demonstrate that EvenNet outperforms full-order models in generalizing across homophilic and heterophilic graphs, implying that ignoring odd-hop neighbors improves the robustness of GNNs. We conduct experiments on both synthetic and real-world datasets to demonstrate the effectiveness of EvenNet. Notably, EvenNet outperforms existing defense models against structural attacks without introducing additional computational costs and maintains competitiveness in traditional node classification tasks on homophilic and heterophilic graphs.

1 Introduction

Graph Neural Networks (GNNs) have gained widespread interest for their excellent performance in graph representation learning tasks [10, 14, 17, 26, 29]. GCN is known to be equivalent to a low-pass filter [2, 21], which leverages the homophily assumption that “connected nodes are more likely to have the same label” as the inductive bias. Such assumptions fail in heterophilic settings [37], where connected nodes tend to have different labels, encouraging research into heterophilic GNNs [1, 22, 37]. Among them, spectral GNNs with learnable polynomial filters [3, 9, 15] adaptively learn suitable graph filters from training graphs and achieve promising performance on both homophilic and heterophilic graphs. If the training graph is heterophilic, a high-pass or composite-shaped graph filter is empirically obtained.

While GNNs are powerful in graph representation learning, recent studies suggest that they are vulnerable to adversarial attacks, where graph structures are perturbed by inserting and removing edges on victim graphs to lower the predictive accuracy of GNNs [38, 31]. Zhu et al. [36] first established the relationship between graph homophily and structural attacks. They claimed that existing attack mechanisms tend to introduce heterophily to homophilic graphs, which significantly degrade the performance of GNNs with low-pass filters. On the one hand, several attempts are made to improve

the robustness of GNNs against the injected heterophily from the spatial domain [12, 16, 30, 34, 35]. These methods either compute edge attention or learn new graph structures with node features, requiring high computational costs in the spatial domain. On the other hand, while spectral GNNs hold superiority on heterophilic graphs, their performance under structural perturbation is unsatisfactory as well, which arouses our interest in exploring the robustness of current spectral methods.

In this study, we consider homophily-heterophily inductive learning tasks, which naturally model non-targeted structural attacks. We observe that structure attacks enlarge the homophily gap between training and test graphs besides introducing heterophily, challenging spectral GNNs to generalize across different homophily levels. Consequently, despite their outstanding performance on heterophilic graphs, spectral GNNs such as GPRGNN have poor generalization ability when the training and test graphs have different homophily. For example, suppose we now have two friend-enemy networks like the ones in Figure 1. If friends are more likely to become neighbors, representing the relationship “like”, the network is homophilic. If enemies form more links corresponding to the relationship “hate”, the network becomes heterophilic. If we apply spectral GNNs trained on “like” networks (where a low-pass filter is obtained) to “hate” networks, we will mistake enemies for friends on “hate” networks. Despite the strength of spectral GNNs in approximating optimal graph filters of arbitrary shapes, the lack of constraints on learned filters makes it difficult for them to generalize.

To improve the performance of current spectral methods against adversarial attacks, we design a novel spectral GNN that realizes generalization across homophily. Our contributions are:

- We proposed EvenNet, a simple yet effective spectral GNN that can be generalized to graphs of different homophily. EvenNet discards messages from odd-order neighbors inspired by balance theory, deriving a graph filter with only even-order terms. We provide a detailed theoretical analysis in the spatial domain to illustrate the advantages of EvenNet in generalizing to graphs of different homophily.
- We propose Spectral Regression Loss (SRL) to evaluate the performance of graph filters on specific graphs in the spectral domain. We theoretically analyze the relationship between graph filters and graph homophily, confirming that EvenNet with symmetric constraints is more robust in homophily-heterophily inductive learning tasks.
- We conduct comprehensive experiments on both synthetic and real-world datasets. The empirical results validate the superiority of EvenNet in generalizing to test graphs of different homophily without introducing additional computational complexity while remaining competitive in traditional node classification tasks.

2 Preliminaries

Notations. Let $\mathcal{G} = (\mathcal{V}, \mathcal{E})$ denote an undirected graph, where $N = |\mathcal{V}|$ is the number of nodes. Let $A \in \{0, 1\}^{N \times N}$ denote the adjacency matrix. Concretely, $A_{ij} = 1$ indicates an edge between nodes v_i and v_j . Graph Laplacian is defined as $L = D - A$, along with a normalized version $\tilde{L} = I - D^{-1/2}AD^{-1/2}$, where I is the identity matrix and D is a diagonal degree matrix with each diagonal element $D_{ii} = \sum_{j=1}^N A_{ij}$. It is known that \tilde{L} is a symmetric positive semidefinite matrix that can be decomposed as $\tilde{L} = U\Lambda U^T$, where $\Lambda = \text{diag}\{\lambda_0, \dots, \lambda_{N-1}\}$ is a diagonal eigenvalue matrix with $0 = \lambda_0 \leq \lambda_1 \leq \dots \leq \lambda_{N-1} \leq 2$, and U is a unitary matrix consisting of eigenvectors.

For multi-class node classification tasks, nodes in \mathcal{G} are divided into K classes $\{\mathcal{C}_0, \dots, \mathcal{C}_{K-1}\}$. Each node v_i is attached with an F dimension feature and a one-hot class label. Let $X \in \mathbb{R}^{N \times F}$ be the input feature matrix and $Y \in \mathbb{R}^{N \times K} = (y_0, \dots, y_{K-1})$ be the label matrix, where y_i is the indicator vector of class \mathcal{C}_i . Let $\mathcal{R} = Y^T Y$ and the size of class \mathcal{C}_k be \mathcal{R}_k .

Graph filtering. The graph filtering operation on graph signal X is defined as $Z = \sigma(Ug(\Lambda)U^T X)$, where $g(\Lambda)$ is the so-called graph filter, and σ is the normalization function. Directly learning

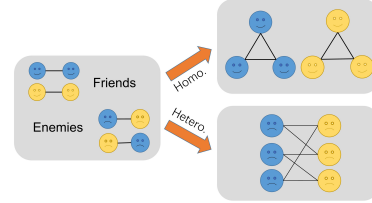


Figure 1: Two friend-enemy networks of opposite homophily.

$g(\Lambda)$ requires eigendecomposition (EVD) of time complexity $O(N^3)$. Recent studies suggest using polynomials to approximate $g(\Lambda)$ instead, which is:

$$Ug(\Lambda)U^T X \approx U \left(\sum_{i=0}^{K-1} w_k \Lambda^k \right) U^T X = \sum_{i=0}^{K-1} w_k \tilde{L}^k X,$$

where $\{w_k\}$ are polynomial coefficients. We can also denote a K -order polynomial graph filter as a filter function $g(\lambda) = \sum_{k=0}^K w_k \lambda^k$ that maps eigenvalue $\lambda \in [0, 2]$ to $g(\lambda)$.

Homophily. Homophily reflects nodes' preferences for choosing neighbors. For a graph of strong homophily, nodes show a tendency to form connections with nodes of the same labels. The ratio of homophily h measures the level of overall homophily in a graph. Several homophily metrics have been proposed with different focuses [20, 22]. We adopt edge homophily following [37], defined by

$$h = \frac{|\{(u, v) : (u, v) \in \mathcal{E} \wedge y_u = y_v\}|}{|\mathcal{E}|}. \quad (1)$$

By definition, $h \in [0, 1]$ is the fraction of intra-class edges in the graph. The closer h is to 1, the more homophilic a graph is.

3 Our Proposed Method: EvenNet

In this section, we first introduce our motivation and the methodology of EvenNet. We then explain how EvenNet enhances the robustness of spectral GNNs from the perspective of both spatial and spectral domains.

3.1 Motivations

Reconsider the toy example in Figure 1. Relationships between nodes are opposite on homophilic and heterophilic graphs, being straightforward but erratic under changes in the graph structure. Unconstrained spectral GNNs tend to overuse such unstable relationships and fail to generalize across homophily. In contrast, a robust model should rely on more general topological information beyond homophily.

Balance theory [6], which arose from signed networks, offers a good perspective: “The enemy of my enemy is my friend, and the friend of my friend is also my friend.” Balance theory always holds as a more general law, regardless of how structural information is revealed on the graph. As a result, we can obtain a more robust spectral GNN under homophily change by incorporating balance theory into graph filter design.

3.2 EvenNet

Denote propagation matrix as $P = I - \tilde{L} = D^{-\frac{1}{2}} A D^{-\frac{1}{2}}$. A K -order polynomial graph filter is defined as $g(\tilde{L}) = \sum_{k=0}^K w_k \tilde{L}^k$, where $w_k, k = 0, \dots, K$ are learnable parameters. We can rewrite the filter as $g(\tilde{L}) = \sum_{k=0}^K w_k (I - \tilde{L})^k = \sum_{k=0}^K w_k P^k$ since w_k is learnable. Then, we discard the monomials in $g(\tilde{L})$ containing odd-order P , obtaining:

$$g_{\text{even}}(\tilde{L}) = \sum_{k=0}^{\lfloor K/2 \rfloor} w_k (I - \tilde{L})^{2k} = \sum_{k=0}^{\lfloor K/2 \rfloor} w_k P^{2k}. \quad (2)$$

In practice, we decouple the transformation of input features and graph filtering process following [9, 18]. Our model then takes the simple form:

$$Z = f(X, P) = \left(\sum_{k=0}^{\lfloor K/2 \rfloor} w_k P^{2k} t(X) \right), \quad (3)$$

where t is an input transformation function (e.g. MLP), and Z is the output node representation that can be fed into a softmax activation function for node classification tasks.

From the perspective of the spectral domain, g_{even} keeps both low and high frequencies components and suppresses medium-frequency components, which is a band-rejection filter with the filter function inherently symmetric about $\lambda = 1$. We provide a theoretical analysis to demonstrate further the advantages of g_{even} in Section 3.3 and 3.4.

3.3 Analysis from the Spatial Domain

Recently, Chen et al. [8] analyzed the performance of graph filters under certain homophily. They concluded that graph filters operate as a potential reconstruction mechanism of the graph structure. A graph filter $g(\tilde{L})$ achieves **better** performance in a binary node classification task when the homophily of the transformed graph is **high**. The transformed homophily can therefore be seen as an indicator of the performance of graph filters on specific tasks. We now provide the well-defined transformed homophily adopted from [8].

Definition 1. (*k-step interaction probability*) For a propagation matrix $P = D^{-\frac{1}{2}}AD^{-\frac{1}{2}}$, the *k-step interaction probability* matrix is

$$\tilde{\Pi}^k = \mathcal{R}^{-\frac{1}{2}}Y^\top P^k Y \mathcal{R}^{-\frac{1}{2}}.$$

Definition 2. (*k-homophily degree*) For a graph \mathcal{G} with the *k-step interaction probability* $\tilde{\Pi}^k$, its *k-homophily degree* $\mathcal{H}_k(\tilde{\Pi})$ is defined as

$$\mathcal{H}_k(\tilde{\Pi}) = \frac{1}{N} \sum_{l=0}^{K-1} \left(\mathcal{R}_l \tilde{\Pi}_l^k - \sum_{m \neq l} \sqrt{\mathcal{R}_m \mathcal{R}_l} \tilde{\Pi}_{lm}^k \right).$$

The transformed 1-homophily degree with filter $g(\tilde{L})$ is $\mathcal{H}_1(g(I - \tilde{\Pi}))$.

By definition, the *k-homophily degree* reflects the average possibility of deriving a node's label from its *k-hop* neighbors. In Theorem 1, we show that even-order filters achieve more robust performance under homophily change by enjoying a lower variance of transformed homophily degree without losing average performance. The detailed proof is provided in Appendix A.1, including discussions about multi-class cases.

Theorem 1. In a binary node classification task, assume the edge homophily $h \in [0, 1]$ is a random variable that belongs to a uniform distribution. An even-order graph filter achieves no less $\mathbb{E}_{\mathcal{H}} \left[\mathcal{H}_1 \left(g(I - \tilde{\Pi}) \right) \right]$ with lower variation than the full-order version.

3.4 Analysis from Spectral Domain

Similar to Section 3.3, we first proposed Spectral regression loss (SRL) as an evaluation metric of graph filters in the spectral domain. In a binary node classification task, suppose the dimension of inputs $F = 1$. Denote the difference of labels as $\Delta y = y_0 - y_1$. A graph filtering operation is defined as $Z = \sigma(Ug(\Lambda)U^\top X)$. Desirable filtering produces distinguishable node representations correlated to Δy to identify node labels. Let $\alpha = U^\top \Delta y$ and $\beta = U^\top X$. The classification task in the spectral domain is then a regression problem in the form of $\sigma(\alpha) = \sigma(g(\Lambda)\beta)$. We adopt Mean Squared Error (MSE) as the objective function of the regression problem and vector normalization as σ . Then SRL is defined as follows:

Definition 3. (*Spectral regression loss*) Denote $\alpha = (\alpha_0, \dots, \alpha_{N-1})^\top$, $\beta = (\beta_0, \dots, \beta_{N-1})^\top$. In a binary node classification task, Spectral Regression Loss (SRL) of filter $g(\Lambda)$ on graph \mathcal{G} is:

$$L(\mathcal{G}) = \sum_{i=0}^{N-1} \left(\frac{\alpha_i}{\sqrt{N}} - \frac{g(\lambda_i)\beta_i}{\sqrt{\sum_{j=0}^{N-1} g(\lambda_j^2)\beta_j^2}} \right)^2 \quad (4)$$

$$= 2 - \frac{2}{\sqrt{N}} \sum_{i=0}^{N-1} \frac{\alpha_i g(\lambda_i)\beta_i}{\sqrt{\sum_{j=0}^{N-1} g(\lambda_j^2)\beta_j^2}}. \quad (5)$$

A graph filter that achieves **lower** SRL is of **higher** performance in the task.

Filters that Minimize SRL. Suppose $\alpha_i = w\beta_i + \epsilon$, where $w > 0$ reflects the correlation between labels and features in the spectral domain and ϵ be the noise term. If ϵ is close to 0, indicating the feature is free of noise and highly predictive, an all-pass filter (for example, MLP) with $g(\lambda_i) = 1$ already minimizes SRL. If the noise becomes dominant, SRL is approximately equal to $\frac{1}{N} \sum_{i=0}^{N-1} (\alpha_i - \frac{g(\lambda_i)}{\sqrt{\sum_j g(\lambda_j)^2}})^2$. In this noise-dominant case, an ideal filter is linearly correlated to α and entirely structure-based to achieve a lower SRL. Most real-world situations lie between these two opposite settings. As a result, the shape of an ideal graph filter lies between an all-pass filter and an α -dependent filter.

From the discussion above, we have shown that the performance of graph filters is related to the correlation between $g(\lambda)$ and α . By connecting α and h in Theorem 2, we establish the relationship between graph homophily and the performance of graph filters.

Theorem 2. *For a binary node classification task on a k -regular graph \mathcal{G} , let h be edge homophily and λ_i be the i -th smallest eigenvalue of \tilde{L} , then*

$$1 - h = \frac{\sum_{i=0}^{N-1} \alpha_i^2 \lambda_i}{2 \sum_{j=0}^{N-1} \lambda_i} \quad (6)$$

The above equation can be extended to general graphs by replacing the normalized Laplacian \tilde{L} with the unnormalized L .

Notice that $\sum_{i=0}^{N-1} \alpha_i^2 \lambda_i$ is a convex combination of non-decreasing $\{\lambda_i\}$ with weights α_i^2 . On a homophilic graph where h is close to 1, the right-hand side of Equation 6 is close to 0, implying larger weights for smaller λ_i . A low-pass filter that suppresses high-frequency components is more correlated with such α and therefore achieves lower SRL. From previous works, we have known that low-pass filters hold superiority on homophilic graphs, which is consistent with our analysis.

In the case of generalization, the distribution of $\{\alpha_i\}$ is not fixed. A graph filter that minimizes the SRL on training graphs could achieve poor results on a test graph of different homophily. Remember that vanilla GCN could be worse than MLP on many heterophilic graphs. The same conclusion can be applied to learnable filters without any constraints, as they only tried to minimize SRL of training graphs. In Theorem 3, we prove that even-order design helps spectral GNNs better generalize between homophilic and heterophilic graphs as a practical constraint to current filters.

Theorem 3. *For a homophilic graph \mathcal{G}_1 with non-increasing $\{\alpha_i\}$ and a heterophilic graph \mathcal{G}_2 with non-decreasing $\{\alpha_i\}$, an even-order filter g_{even} that is trained on one of the graphs achieves a lower SRL gap $|L(\mathcal{G}_1) - L(\mathcal{G}_2)|$ when generalized to the other graph than a trained full-order filter.*

Theorem 3 reveals a trade-off in filter design between fitting the training graph and generalizing across graphs of different homophily. While naive low-pass filters and high-pass filters work better on graphs with certain homophily, EvenNet tolerates imperfect filter learning and becomes more robust under homophily changes. A specific example of ring graphs is given in the following proposition. We see that EvenNet intrinsically satisfies the necessary condition for perfect generalization.

Proposition 1. *Consider two ring graphs \mathcal{G}_1 and \mathcal{G}_2 of $2n$ nodes, $n \in \mathbb{N}^+$. Suppose $h(\mathcal{G}_1) = 0$ and $h(\mathcal{G}_2) = 1$. Assume the spectrum of input difference $\beta = c\mathbf{1}$, where $c > 0$ is a constant. Then the necessary condition for a graph filter $g(\lambda)$ to achieve $L(\mathcal{G}_1) = L(\mathcal{G}_2)$ is $g(0) = g(2)$.*

4 Related Work

Spectral GNNs. GNNs have become prevalent in graph representation learning tasks. Among them, Spectral GNNs focus on designing graph filters with filter functions that operate on eigenvalues of graph Laplacian [5]. Graph filters could be fixed [17, 18, 29] or approximated with polynomials. ChebNet [10] adopts Chebyshev polynomials to realize faster localized spectral convolution. ARMA [3] achieves a more flexible filter approximation with Auto-Regressive Moving Average filters. GPRGNN [9] connects graph filtering with graph diffusion and learns coefficients of polynomial filters directly. BernNet [15] utilizes Bernstein approximation to learn arbitrary filtering functions. Although learnable graph filters perform well on heterophilic graphs, they have difficulties generalizing if a homophily gap exists between training and test graphs.

GNNs for Heterophily. Previous works pointed out the weakness of vanilla GCN on graphs with heterophily. Recently, various GNNs have been proposed to tackle this problem. Geom-GCN [22] uses a novel neighborhood aggregation scheme to capture long-distance information. Zhu et al. [37] introduce several designs that are helpful for GNNs to learn representations beyond homophily. FAGCN [4] adaptively combines signals of different frequencies in message passing via a self-gating mechanism. While these methods can handle heterophilic graphs, they are not guaranteed to generalize across graphs of different homophily.

Robust GNNs. In the field of designing robust GNNs, existing methods can be divided into two main categories: **1) Models utilizing new graph structures.** GNN-Jaccard [30] and GNN-SVD [12] preprocess the input graph before applying vanilla GCN. ProGNN [16] jointly learns a better graph structure and a robust model. **2) Attention-based models.** RGCN [35] uses variance-based attention to evaluate the credibility of nodes’ neighbors. GNNGuard [34] adopts neighbor importance estimation, aligning higher scores to trustworthy neighbors. TWIRLS [32] applies an attention mechanism inspired by classical iterative methods PGD and IRLS. These methods are effective against structural attacks. However, the learned graph structure cannot be applied to inductive learning settings and requires additional memory. At the same time, attention-based models are limited in the spatial domain and need high computational costs. On the contrary, EvenNet improves the robustness of spectral GNNs without introducing additional computational costs.

5 Experiment

We conduct three experiments to test the ability of EvenNet in (1) generalizing across homophily on synthetic datasets, (2) defending against non-targeted structural attacks, and (3) supervised node classification on real-world datasets.

5.1 Baselines

We compare our EvenNet with the following methods. (1) Method only using node features: A 2-layer MLP. (2) Methods achieving promising results on homophilic graphs: GCN [17], GAT [26], GCNII [7]. (3) Methods handling heterophilic settings: H2GCN [37], FAGCN [4], GPRGNN [9]. We also include five advanced defense models in the experiment about adversarial attacks, including RobustGCN [35], GNN-SVD [12], GNN-Jaccard [30], GNNGuard [34], and ProGNN [16]. We implement the above models with the help of PyTorch Geometric [13] and DeepRobust libraries [19]. Details about hyperparameters and network architectures are deferred to Appendix C.2.

5.2 Evaluation on synthetic datasets

Datasets. In the first experiment testing generalization ability, we use cSBM model to generate graphs with arbitrary homophily levels following [9]. Specifically, we divide nodes into two classes of equal size. Each node is attached with a feature vector randomly sampled from a class-specific Gaussian distribution. The homophily level of a graph is controlled by parameter $\phi \in [-1, 1]$. A larger $|\phi|$ indicates that the generated graph provides stronger topological information, while $\phi = 0$ means only node features are helpful for prediction. Note that if $\phi > 0$, the graph is more homophilic and vice versa. Details about cSBM dataset are left to Appendix B.2.

Settings. We set up node classification tasks in the inductive setting. We generate three graphs of the same size for each sub-experiment, one graph each for training, validation, and testing. Graphs for validation and testing share the same ϕ_{test} , while training graphs either take $\phi_{train} = \phi_{test}$ or $\phi_{train} = -\phi_{test}$. If $\phi_{train} = -\phi_{test}$, the training and test graphs are of opposite homophily but provide the same amount of topological information. A model manages to generalize across homophily when it realizes high prediction accuracy in both scenarios. In practice, we choose $(\phi_{train}, \phi_{test}) \in \{(\pm 0.5, \pm 0.5), (\pm 0.75, \pm 0.75)\}$.

Results. The results are presented in Table 1. When $\phi_{train} = \phi_{test}$, GPRGNN achieves the highest predictive accuracy as it best fits the desired graph filter. However, when $\phi_{train} = -\phi_{test}$, all methods except EvenNet suffer from a huge performance drop. Vanilla GCN, which corresponds to a low-pass filter, achieves desirable performance only when the test graph is homophilic. GPRGNN overfits training graphs most, resulting in more severe performance degradation on test graphs of

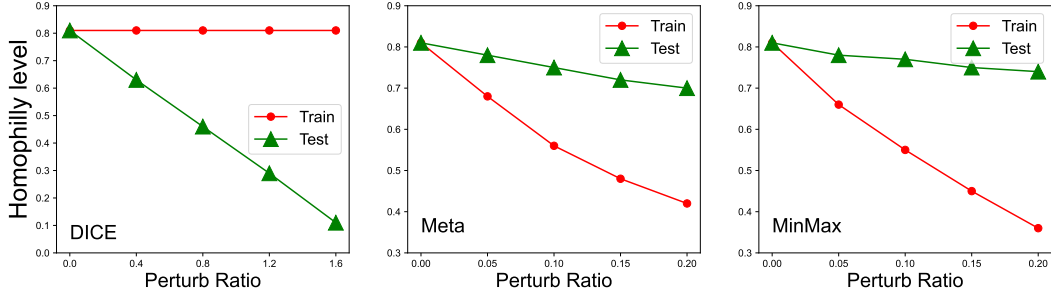


Figure 2: Homophily level of training graphs and test graphs on Cora after DICE attack, Metattack and MinMax attack. All attacks result in homophily gap between training and test graphs.

opposite homophily. EvenNet is the only method that achieves more than 75% accuracy on all datasets among all the models, which is robust in generalization across homophily.

Table 1: Average node classification accuracy(%) and absolute performance gap(%) between experiments of the same ϕ_{train} over ten repeated experiments on synthetic cSBM datasets. The best result is highlighted by **bold** font, the second best result is underlined.

ϕ_{train}	0.75		0.50		-0.50		-0.75					
ϕ_{test}	0.75	-0.75	gap(\downarrow)	0.50	-0.50	gap(\downarrow)	-0.50	0.50	gap(\downarrow)	-0.75	0.75	gap(\downarrow)
MLP	57.92	57.24	0.68	63.65	64.26	0.61	63.28	63.83	0.55	56.92	59.24	<u>2.32</u>
GCN	75.24	60.31	15.11	78.98	63.21	15.77	63.27	76.67	13.40	60.48	<u>77.88</u>	17.40
GAT	74.15	<u>60.55</u>	13.60	75.64	61.96	13.68	64.43	71.02	6.59	63.19	71.61	8.42
GCNII	83.12	54.30	28.82	78.07	58.43	19.64	72.32	67.68	4.64	65.93	62.92	3.01
H2GCN	76.41	54.81	21.60	78.86	58.89	19.97	78.43	59.77	18.66	76.29	55.92	20.37
FAGCN	81.29	60.44	20.85	78.73	60.28	18.45	79.45	60.62	18.83	85.78	57.34	28.44
GPRGNN	95.93	53.52	42.41	84.42	56.16	28.26	84.18	63.76	20.42	95.99	66.49	29.52
EvenNet	<u>95.29</u>	94.59	0.70	<u>82.37</u>	82.57	0.20	<u>81.99</u>	79.81	<u>2.18</u>	<u>94.79</u>	96.25	1.46

5.3 Performance under non-targeted structural adversarial attacks

Datasets. For adversarial attacks, we use four public graphs, Cora, Citeseer, PubMed [24, 33] and ACM [27] available in DeepRobust Library [19]. We use the same preprocessing method and splits as [38], where the node set is split into 10% for training, 10% for validation, and 80% for testing.

Attack methods. Graph structural attacks can be categorized into poison attacks and evasion attacks. In poison attacks, attack models are trained to lower the performance of a surrogate GNN model. The training graph and the test graph are both allowed to be perturbed but only with a limited amount of modifications, which are referred to as perturb ratios. Evasion attacks only happen during the inference phase, which means GNNs are trained on clean graphs. In our study, we include two poison attacks, Metattack (Meta) [38] and MinMax attack [31] with GCN the surrogate model, and an evasion variant of DICE attack [28]. For poison attacks, we use the same setting in [34] and set the perturb ratio for poison attacks to be 20%. For the evasion DICE, we randomly remove intra-class edges and add inter-class edges on the test graph while keeping the graph structure between labeled nodes unchanged. We set the perturb ratio of DICE attack in $\{0.4, 0.8, 1.2, 1.6\}$. From Figure 2, it can be seen that all attacks result in homophily gaps between training graphs and the test graphs.

Results. Defense results are presented in Table 2 and Figure 3. For DICE attack, the performance of all methods significantly decreases along with the increase of homophily gap except EvenNet. Interestingly, when the homophily gap is enormous, EvenNet enjoys a performance rebound, consistent with our topological information theory (strong homo. and strong hetero. are both helpful for prediction). For poison attacks, EvenNet achieves five SOTA compared with advanced defense models. Unlike spatial defense models, EvenNet is free of introducing extra time or space complexity.

Table 2: Average node classification accuracy (%) against non-targeted poison attacks Metattack and MinMax attack with perturb ratio 20% over 5 different splits. The best result is highlighted by **bold** font, the second best result is underlined.

Dataset	Meta-cora	Meta-citeseer	Meta-acm	MM-cora	MM-citeseer	MM-acm
MLP	58.60	62.93	85.74	59.81	63.72	<u>85.66</u>
GCN	63.76	61.98	68.29	69.21	68.02	<u>69.37</u>
GAT	66.51	63.66	68.50	69.50	67.04	69.26
GCNII	66.57	64.23	78.53	73.01	72.26	82.90
H2GCN	71.62	67.26	83.75	66.76	69.66	84.84
FAGCN	72.14	66.59	85.93	64.90	66.33	81.49
GPRGNN	69.08	65.63	<u>86.23</u>	77.33	72.21	83.64
RobustGCN	60.38	60.44	62.29	68.53	63.16	61.60
GNN-SVD	64.83	64.98	84.55	66.33	64.97	81.08
GNN-Jaccard	68.30	63.40	67.81	72.98	68.43	69.03
GNNGuard	<u>75.98</u>	68.57	62.19	73.23	66.14	66.15
ProGNN	75.25	68.15	83.99	<u>77.91</u>	<u>72.26</u>	73.51
EvenNet	76.26	<u>68.54</u>	89.55	78.42	73.98	87.35

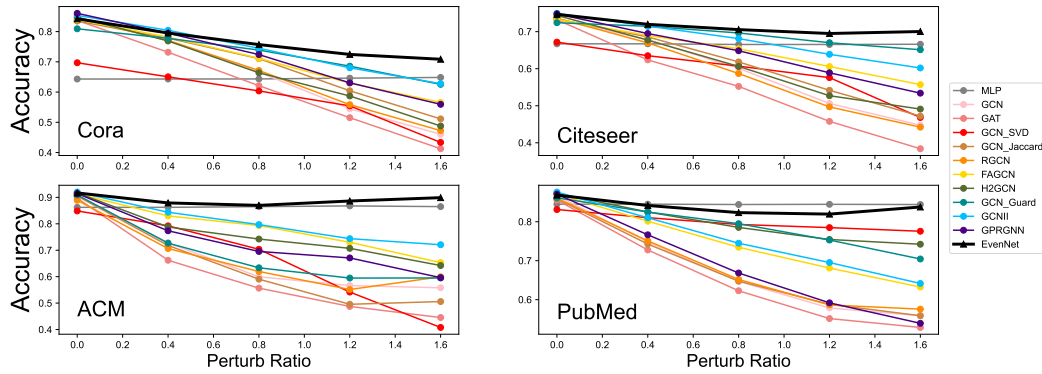


Figure 3: DICE attack on four homophilic datasets. EvenNet is marked with “ \triangle ”.

5.4 Performance on real-world graph datasets

We evaluate EvenNet on real-world datasets to examine the performance of EvenNet on clean graphs. Besides of the datasets used in Section 5.3, we additionally include four public heterophilic datasets: Actor, Cornell, Squirrel and Texas [22, 23, 25]. For all datasets, we adopt dense splits the same as [22] to perform full-supervised node classification tasks, where the node set is split into 60% for training, 20% for validation, and 20% for testing. The results are shown in Table 3. While EvenNet sacrifices its performance for robustness, it is still competitive on most datasets.

5.5 Ablation study

To analyze the effect of introducing odd-order components into graph filters, we develop a regularized variant of EvenNet named EvenReg. EvenReg adopts a full-order learnable graph filter, with the coefficients of odd-order monomials being punished as a regularization term. The training loss of EvenReg then takes the form: $\mathcal{L} = \mathcal{L}_{pred} + \eta \sum_{k=0}^{[K/2]} |w_{2k+1}|$, where \mathcal{L}_{pred} is the classification loss and η is a hyper-parameter controlling the degree of regularization.

We set $\eta = 0.05$ and repeat experiments in Section 5.2. The results are presented in Table 4. The performance of EvenReg lies between full-order GPRGNN and EvenNet, indicating the introduced odd orders impede spectral GNNs to generalize across homophily.

Table 3: Average node classification accuracy(%) on real-world benchmark datasets over 10 different splits. The best result is highlighted by **bold** font, the second best result is underlined.

Model	Cora	Cite.	Pubm.	Cham.	Texas	Corn.	Squi.	Actor
MLP	74.88	74.82	85.58	46.65	89.50	90.17	32.33	41.30
GCN	87.19	80.87	87.51	63.28	80.66	74.09	46.42	34.21
GAT	88.21	<u>81.36</u>	89.42	64.02	81.63	81.97	47.87	36.21
GCNII	87.91	82.13	86.41	50.76	86.23	89.83	36.35	<u>41.68</u>
FAGCN	88.83	80.35	89.34	56.67	89.18	90.16	39.10	41.18
H2GCN	87.59	79.69	88.68	55.88	88.52	85.57	34.45	39.62
GPRGNN	<u>88.34</u>	80.16	90.08	67.13	<u>93.44</u>	92.45	51.93	41.62
EvenNet	87.25	79.67	<u>89.52</u>	<u>66.13</u>	93.77	<u>92.13</u>	<u>49.80</u>	41.69

Table 4: Average node classification accuracy(%) of EvenReg over 10 repeated experiments on synthetic cSBM datasets.

ϕ_{train}	0.75		0.50		-0.50		-0.75	
ϕ_{test}	0.75	-0.75	0.50	-0.50	-0.50	0.50	-0.75	0.75
GPRGNN	95.93	53.52	84.42	56.16	84.18	63.76	95.99	66.49
EvenNet	95.29	94.59	82.37	82.57	81.99	79.81	94.79	96.25
EvenReg	95.44	93.90	84.05	78.06	83.72	75.33	95.40	95.73

6 Conclusion

In this study, we investigate the ability of current GNNs to generalize across homophily. We observe that all existing methods experience severe performance degradation if a large homophily gap exists between training and test graphs. To overcome this difficulty, we proposed EvenNet, a simple yet effective spectral GNN robust under homophily change of graphs. We provide a detailed theoretical analysis to illustrate the advantages of EvenNet in generalization. We conduct experiments on both synthetic and real-world datasets. The empirical results verify the superiority of EvenNet in inductive learning across homophily and defense under structural attacks by sacrificing only a tiny amount of predictive accuracy on clean graphs.

References

- [1] Sami Abu-El-Haija, Bryan Perozzi, Amol Kapoor, Hrayr Harutyunyan, Nazanin Alipourfard, Kristina Lerman, Greg Ver Steeg, and Aram Galstyan. Mixhop: Higher-order graph convolutional architectures via sparsified neighborhood mixing. In *ICML*, 2019. 1
- [2] Muhammet Balcilar, Guillaume Renon, Pierre Héroux, Benoit Gaüzère, Sébastien Adam, and Paul Honeine. Analyzing the expressive power of graph neural networks in a spectral perspective. In *ICLR*, 2020. 1
- [3] Filippo Maria Bianchi, Daniele Grattarola, Lorenzo Livi, and Cesare Alippi. Graph neural networks with convolutional arma filters. In *TPAMI*, 2021. 1, 4
- [4] Deyu Bo, Xiao Wang, Chuan Shi, and Huawei Shen. Beyond low-frequency information in graph convolutional networks. In *AAAI*, 2021. 4, 5.1
- [5] Joan Bruna, Wojciech Zaremba, Arthur Szlam, and Yann LeCun. Spectral networks and locally connected networks on graphs. In *ICLR*, 2014. 4
- [6] Dorwin Cartwright and Frank Harary. Structural balance: a generalization of heider’s theory. *Psychological review*, 63(5):277, 1956. 3.1
- [7] Ming Chen, Zhewei Wei, Zengfeng Huang, Bolin Ding, and Yaliang Li. Simple and deep graph convolutional networks. In *ICML*, 2020. 5.1
- [8] Zhixian Chen, Tengfei Ma, and Yang Wang. When does a spectral graph neural network fail in node classification? *arXiv preprint arXiv:2202.07902*, 2022. 3.3

- [9] Eli Chien, Jianhao Peng, Pan Li, and Olgica Milenkovic. Adaptive universal generalized pagerank graph neural network. In *ICLR*, 2021. 1, 3.2, 4, 5.1, 5.2, B.1, B.2
- [10] Michaël Defferrard, Xavier Bresson, and Pierre Vandergheynst. Convolutional neural networks on graphs with fast localized spectral filtering. In *NIPS*, 2016. 1, 4
- [11] Yash Deshpande, Subhabrata Sen, Andrea Montanari, and Elchanan Mossel. Contextual stochastic block models. In *NIPS*, 2018. B.2
- [12] Negin Entezari, Saba A Al-Sayouri, Amirali Darvishzadeh, and Evangelos E Papalexakis. All you need is low (rank): Defending against adversarial attacks on graphs. In *WSDM*, 2020. 1, 4, 5.1
- [13] Matthias Fey and Jan Eric Lenssen. Fast graph representation learning with pytorch geometric. In *ICLR*, 2019. 5.1, C.2
- [14] William L. Hamilton, Zhitao Ying, and Jure Leskovec. Inductive representation learning on large graphs. In *NIPS*, 2017. 1
- [15] Mingguo He, Zhewei Wei, Zengfeng Huang, and Hongteng Xu. Bernnet: Learning arbitrary graph spectral filters via bernstein approximation. In *NIPS*, 2021. 1, 4
- [16] Wei Jin, Yao Ma, Xiaorui Liu, Xianfeng Tang, Suhang Wang, and Jiliang Tang. Graph structure learning for robust graph neural networks. In *SIGKDD*, 2020. 1, 4, 5.1
- [17] Thomas N. Kipf and Max Welling. Semi-supervised classification with graph convolutional networks. In *ICLR*, 2017. 1, 4, 5.1
- [18] Johannes Klicpera, Aleksandar Bojchevski, and Stephan Günnemann. Predict then propagate: Combining neural networks with personalized pagerank for classification on graphs. In *ICLR*, 2018. 3.2, 4
- [19] Yixin Li, Wei Jin, Han Xu, and Jiliang Tang. Deeprobust: A pytorch library for adversarial attacks and defenses. *arXiv preprint arXiv:2005.06149*, 2020. 5.1, 5.3, C.2
- [20] Derek Lim, Felix Hohne, Xiuyu Li, Sijia Linda Huang, Vaishnavi Gupta, Omkar Bhalerao, and Ser Nam Lim. Large scale learning on non-homophilous graphs: New benchmarks and strong simple methods. In *NIPS*, 2021. 2, C.2
- [21] Hoang Nt and Takanori Maehara. Revisiting graph neural networks: All we have is low-pass filters. *arXiv: Machine Learning*, 2019. 1
- [22] Hongbin Pei, Bingzhe Wei, Kevin Chen-Chuan Chang, Yu Lei, and Bo Yang. Geom-gcn: Geometric graph convolutional networks. In *ICLR*, 2020. 1, 2, 4, 5.4
- [23] Benedek Rozemberczki, Carl Allen, and Rik Sarkar. Multi-scale attributed node embedding. In *Journal of Complex Networks*, 2021. 5.4
- [24] Prithviraj Sen, Galileo Namata, Mustafa Bilgic, Lise Getoor, Brian Galligher, and Tina Eliassi-Rad. Collective classification in network data. In *AI magazine*, 2008. 5.3
- [25] Jie Tang, Jimeng Sun, Chi Wang, and Zi Yang. Social influence analysis in large-scale networks. In *SIGKDD*, 2009. 5.4
- [26] Petar Velickovic, Guillem Cucurull, Arantxa Casanova, Adriana Romero, Pietro Liò, and Yoshua Bengio. Graph attention networks. In *ICLR*, 2018. 1, 5.1
- [27] Xiao Wang, Houye Ji, Chuan Shi, Bai Wang, Yanfang Ye, Peng Cui, and Philip S. Yu. Heterogeneous graph attention network. In *WWW*, 2019. 5.3
- [28] Marcin Waniek, Tomasz Michalak, Talal Rahwan, and Michael Wooldridge. Hiding individuals and communities in a social network. In *Nature Human Behaviour*, 2016. 5.3
- [29] Felix Wu, Amauri Holanda de Souza, Tianyi Zhang, Christopher Fifty, Tao Yu, and Kilian Q. Weinberger. Simplifying graph convolutional networks. In *ICML*, 2019. 1, 4
- [30] Huijun Wu, Chen Wang, Yuriy Tyshetskiy, Andrew Docherty, Kai Lu, and Liming Zhu. Adversarial examples for graph data: Deep insights into attack and defense. In *IJCAI*, 2019. 1, 4, 5.1
- [31] Kaidi Xu, Hongge Chen, Sijia Liu, Pin-Yu Chen, Tsui-Wei Weng, Mingyi Hong, and Xue Lin. Topology attack and defense for graph neural networks: An optimization perspective. In *IJCAL*, 2019. 1, 5.3
- [32] Yongyi Yang, Tang Liu, Yangkun Wang, Jinjing Zhou, Quan Gan, Zhewei Wei, Zheng Zhang, Zengfeng Huang, and David Wipf. Graph neural networks inspired by classical iterative algorithms. In *ICML*, 2021. 4
- [33] Zhilin Yang, William Cohen, and Ruslan Salakhudinov. Revisiting semi-supervised learning with graph embeddings. In *ICML*, 2016. 5.3
- [34] Xiang Zhang and Marinka Zitnik. Gnnguard: Defending graph neural networks against adversarial attacks. In *NIPS*, 2020. 1, 4, 5.1, 5.3

- [35] Dingyuan Zhu, Ziwei Zhang, Peng Cui, and Wenwu Zhu. Robust graph convolutional networks against adversarial attacks. In *KDD*, 2019. 1, 4, 5.1
- [36] Jiong Zhu, Junchen Jin, Donald Loveland, Michael T Schaub, and Danai Koutra. On the relationship between heterophily and robustness of graph neural networks. *arXiv preprint arXiv:2106.07767*, 2021. 1
- [37] Jiong Zhu, Yujun Yan, Lingxiao Zhao, Mark Heimann, Leman Akoglu, and Danai Koutra. Beyond homophily in graph neural networks: Current limitations and effective designs. In *NIPS*, 2020. 1, 2, 4, 5.1, A.1
- [38] Daniel Zügner and Stephan Günnemann. Adversarial attacks on graph neural networks via meta learning. In *ICLR*, 2019. 1, 5.3, B.1

A Additional proofs

A.1 Proof of Theorem 1

Before proving Theorem 1, We first demonstrate the superiority of even-hop neighbors over odd-hop neighbors from the perspective of random walks.

In a binary node classification task, denote the probability of a random walk of length k that starts and ends with nodes of the same label as p_k , $k > 0$. Suppose the edge homophily level h is a random variable that belongs to a uniform distribution in $[0, 1]$ and $p_1 = h$, then:

Lemma 1. *If k is odd, $\mathbb{E}_h[p_k] = \frac{1}{2}$. If k is even, $\mathbb{E}_h[p_k] \geq \frac{1}{2}$.*

Proof. If $k = 1$, $p_1 = h$, $\mathbb{E}_h[p_1] = \mathbb{E}_h[h] = \frac{1}{2}$. If $k = 2$, $p_2 = h^2 + (1-h)^2 = 2(h - \frac{1}{2})^2 + \frac{1}{2} \geq \frac{1}{2}$, $\mathbb{E}_h[p_2] = \int_0^1 p_2 dh \geq \frac{1}{2}$.

For $k > 2$,

$$\begin{aligned} p_k &= p_{k-2} \left((1-h)^2 + h^2 \right) + (1-p_{k-2}) (2h(1-h)) \\ &= 4p_{k-2}h^2 - 4p_{k-2}h + p_{k-2} - 2h^2 + 2h \\ \mathbb{E}_h[p_k] &= \mathbb{E}_h[\mathbb{E}_h[p_k | p_{k-2}]] \\ &= \mathbb{E}_h \left[\int_0^1 p_k dh \right] \\ &= \mathbb{E}_h \left[\frac{1}{3}p_{k-2} + \frac{1}{3} \right] \\ &= \frac{1}{3}(\mathbb{E}_h[p_{k-2} + 1]) \end{aligned}$$

That is, for $\mathbb{E}_h[p_{k-2}] = \frac{1}{2}$, $\mathbb{E}_h[p_k] = \frac{1}{2}$; for $\mathbb{E}_h[p_{k-2}] \geq \frac{1}{2}$, $\mathbb{E}_h[p_k] \geq \frac{1}{2}$. Therefore, Lemma 1 is proved. \square

Multi-class Cases. We now provide a brief discussion of the superiority of even-hop neighbors in multi-class node classification tasks following [37].

Definition 4. *Matrix $Q \in \mathbb{R}^{K \times K}$ is an independent between-class random walk matrix if it holds the following properties:*

- Q is a random walk matrix.
- $\forall i \neq j$, $Q_{ii} = Q_{jj}$.
- $\forall i \neq j, m \neq n$, $Q_{ij} = Q_{mn}$.

Suppose there are K classes of nodes in the graph, where the number of nodes of each class is the same, and node labels are assigned independently. Denote h as the edge homophily level, the 1-step between-class random walk matrix P is in the form of:

$$P = \begin{bmatrix} h & \frac{1-h}{K-1} & \cdots & \frac{1-h}{K-1} \\ \frac{1-h}{K-1} & h & \cdots & \frac{1-h}{K-1} \\ \vdots & \vdots & \ddots & \vdots \\ \frac{1-h}{K-1} & \frac{1-h}{K-1} & \cdots & h \end{bmatrix},$$

where P_{ij} denotes the probability of a 1-step random walk that start with a node of label i and ends with a node of label j . By definition, P is an independent between-class random walk matrix.

Lemma 2. *If $M \in \mathbb{R}^{K \times K}$ is an independent between-class random walk matrix, $P' = MP$ is an independent between-class random walk matrix as well.*

Proof. It can be verified that P' is still a random walk matrix, and for all $i \neq j, m \neq n$:

$$\begin{aligned} P'_{ii} &= \sum_{m=0}^{K-1} M_{im} P_{mi} = \sum_{m=0}^{K-1} M_{jm} P_{mj} = P'_{jj} \\ P'_{ij} &= \sum_{k=0}^{K-1} M_{ik} P_{kj} = \sum_{k=0}^{K-1} M_{mk} P_{kn} = P'_{mn} \end{aligned}$$

By definition, P' is an independent between-class random walk matrix. \square

Denote the k -step between-class random walk matrix as P^k . From Lemma 2, we can conclude that P^k is an independent between-class random walk matrix for all $k \in \mathbb{N}^+$. In Lemma 3, we illustrate the advantages of even-order propagation by comparing the interaction probability between classes.

Lemma 3. *If k is even, the intra-class interaction probability P_{ii}^k is no less than inter-class interaction probability $P_{ij}^k, i \neq j$.*

Proof. For $k = 2$:

$$\begin{aligned} P_{ii}^2 &= h^2 + \frac{(1-h)^2}{K-1} \\ P_{ij}^2 &= \frac{2h(1-h)}{K-1} + \frac{(K-2)(1-h)^2}{(K-1)^2} \\ P_{ii}^2 - P_{ij}^2 &= \left(h - \frac{1-h}{K-1} \right)^2 \geq 0 \end{aligned}$$

The inequality is tight when $h = \frac{1-h}{K-1}$.

For $k = 2m, m > 1, m \in \mathbb{N}^+$, P^m is an independent between-class random walk matrix that can be written as:

$$P^m = \begin{bmatrix} h' & \frac{1-h'}{K-1} & \cdots & \frac{1-h'}{K-1} \\ \frac{1-h'}{K-1} & h' & \cdots & \frac{1-h'}{K-1} \\ \vdots & \vdots & \ddots & \vdots \\ \frac{1-h'}{K-1} & \frac{1-h'}{K-1} & \cdots & h' \end{bmatrix},$$

The above proof for $k = 2$ can be generalized to all $h \in [0, 1]$. Therefore, $P_{ii}^m \geq P_{ij}^m$ is satisfied as well. \square

Note that Lemma 3 is not satisfied for odd k if h is relatively smaller than $\frac{1-h}{K-1}$.

Proof of Theorem 1

Proof. According to Definition 2, for a graph \mathcal{G} with the k -step interaction probability $\tilde{\Pi}^k$, its k -homophily degree $\mathcal{H}_k(\tilde{\Pi})$ is defined as

$$\mathcal{H}_k(\tilde{\Pi}) = \frac{1}{N} \sum_{l=0}^{K-1} \left(\mathcal{R}_l \tilde{\Pi}_{ll}^k - \sum_{m \neq l} \sqrt{\mathcal{R}_m \mathcal{R}_l} \tilde{\Pi}_{lm}^k \right).$$

The transformed 1-homophily degree with filter $g(\tilde{L})$ is $\mathcal{H}_1(g(I - \tilde{\Pi}))$.

Specifically, in a binary node classification problem, the k -homophily degree is:

$$\mathcal{H}_k(\tilde{\Pi}) = \frac{1}{N} \left(\mathcal{R}_0 \tilde{\Pi}_{00}^k + \mathcal{R}_1 \tilde{\Pi}_{11}^k - 2\sqrt{\mathcal{R}_0 \mathcal{R}_1} \tilde{\Pi}_{01}^k \right)$$

Denote a k -order polynomial graph filter as $g_k(\tilde{L}) = w_0 + w_1 \tilde{L} + \dots + w_k \tilde{L}^k$,

Let \tilde{P}_{i00} The transformed 1-homophily degree of $g_k(\tilde{L})$ is:

$$\begin{aligned}
\mathcal{H}_1 \left(g_k(I - \tilde{\Pi}) \right) &= \frac{1}{N} \left(\mathcal{R}_0 g_k \left(I - \tilde{\Pi} \right)_{00} + \mathcal{R}_1 g_k \left(I - \tilde{\Pi} \right)_{11} - 2\sqrt{\mathcal{R}_0 \mathcal{R}_1} g_k \left(I - \tilde{\Pi} \right)_{01} \right) \\
&= \frac{(\sqrt{\mathcal{R}_0} - \sqrt{\mathcal{R}_1})^2}{N} (w_0 + \dots + w_k) \\
&\quad - \frac{\mathcal{R}_0 \tilde{\Pi}_{00} + \mathcal{R}_1 \tilde{\Pi}_{11} - 2\sqrt{\mathcal{R}_0 \mathcal{R}_1} \tilde{\Pi}_{01}}{N} (w_1 + 2w_2 + \dots + kw_k) \\
&\quad + \frac{\mathcal{R}_0 \tilde{\Pi}_{00}^2 + \mathcal{R}_1 \tilde{\Pi}_{11}^2 - 2\sqrt{\mathcal{R}_0 \mathcal{R}_1} \tilde{\Pi}_{01}^2}{N} (w_2 + 3w_3 + \dots) \\
&\quad - \dots \\
&= c - \mathcal{H}_1(\tilde{\Pi})(w_1 + 2w_2 + \dots + kw_k) + \mathcal{H}_2(\tilde{\Pi})(w_2 + 3w_3 + \dots) + \dots \\
&= c + \sum_{i=1}^k \theta_i \mathcal{H}_i(\tilde{\Pi}),
\end{aligned}$$

where c is a constant and each θ_i is a linear sum of $\{w_i\}$ that for arbitrary $x \in \mathbb{R}$:

$$\sum_{i=0}^k \theta_i x^i = \sum_{i=0}^k w_i (1-x)^i.$$

Following Lemma 1, the average possibility of deriving a node's label from its odd-hop neighbors is $\frac{1}{2}$, which means $\mathbb{E}_h[\mathcal{H}_i(\tilde{\Pi})] = 0$ and $\text{Var}_h[\mathcal{H}_i(\tilde{\Pi})] \geq 0$ for odd i . By removing the odd-order terms, the transformed 1-homophily degree does not decrease on average, but enjoys a lower variation.

Rewrite filter $g_k(\tilde{L})$ as $g_k(\tilde{L}) = \theta_0 + \theta_1(I - \tilde{L}) + \dots + \theta_k(I - \tilde{L})^k$ and set $\theta_i = 0$ for odd i , the graph filter is then in the form of :

$$g_k(\tilde{L}) = \sum_{i=0}^{\lfloor k/2 \rfloor} \theta_i (I - \tilde{L})^{2i} = \sum_{i=0}^{\lfloor k/2 \rfloor} \theta_i P^{2i},$$

which is exactly the graph filter of EvenNet. Therefore, EvenNet has lower variation on the transformed 1-homophily degree without sacrificing the average performance.

□

A.2 Proof of Theorem 1

Lemma 4. Given **unnormalized graph Laplacian** $L = U_L \Lambda_L U_L^\top$ and its eigenvalues $\{\lambda'_i\}$, denote the number of edges on the graph is m , and label difference as $\Delta \mathbf{y} = \mathbf{y}_0 - \mathbf{y}_1 \in \mathbb{R}^{N \times 1}$. For **unnormalized** spectrum of label difference on L is $\alpha' = U_L^\top \Delta \mathbf{y} = (\alpha'_0, \alpha'_1, \dots, \alpha'_{N-1})^\top$, then

$$\begin{aligned}
\sum_{i=0}^{N-1} \lambda'_i &= 2m & (7) \\
1 - h &= \frac{\sum_{i=0}^{N-1} (\alpha'_i)^2 \lambda'_i}{2 \sum_{j=0}^{N-1} \lambda'_j}
\end{aligned}$$

Proof. Denote the trace of a matrix M as $\text{tr}(M)$, the degree of node v_i as d_i .

$$\sum_{i=0}^{N-1} \lambda'_i = \text{tr}(L) = \sum_{i=0}^{N-1} d_i = 2m$$

The Dirichlet energy of the label difference is defined as:

$$\begin{aligned}
E(\Delta \mathbf{y}) &= \Delta \mathbf{y}^\top L \Delta \mathbf{y} \\
&= \sum_{(i,j) \in \mathcal{E}} (\Delta \mathbf{y}_i - \Delta \mathbf{y}_j)^2 \\
&= 4 \sum_{(i,j) \in \mathcal{E}} \mathbf{1}\{\Delta \mathbf{y}_i \neq \Delta \mathbf{y}_j\} \\
&= 4(1-h)m
\end{aligned} \tag{8}$$

Using $L = U_L \Lambda_L U_L^\top$, the Dirichlet energy of the label difference can also be expressed as:

$$\begin{aligned}
E(\Delta \mathbf{y}) &= \Delta \mathbf{y}^\top U_L \Lambda_L U_L^\top \Delta \mathbf{y} \\
&= \boldsymbol{\alpha}'^\top \Lambda_L \boldsymbol{\alpha}' \\
&= \sum_{i=0}^{N-1} \lambda'_i (\alpha'_i)^2
\end{aligned} \tag{9}$$

By integrating equations 7 8 9, we get:

$$1-h = \frac{\sum_{i=0}^{N-1} (\alpha'_i)^2 \lambda'_i}{2 \sum_{j=0}^{N-1} \lambda'_j}$$

□

Proof of Theorem 2

Proof. For a k -regular graph, denote normalized graph Laplacian as $\tilde{L} = U \Lambda U^\top$, then

$$\begin{aligned}
\tilde{L} &= D^{-1/2} L D^{-1/2} \\
&= D^{-1/2} U_L \Lambda_L U_L^\top D^{-1/2} \\
&= \frac{1}{k} U_L \Lambda_L U_L^\top
\end{aligned} \tag{10}$$

From equation 10, we get $U = U_L$, $\lambda_i = \lambda'_i/k$. Denote the spectrum of label difference on \tilde{L} as $\boldsymbol{\alpha}$, then $\boldsymbol{\alpha} = \boldsymbol{\alpha}'$. By substituting λ'_i with $k\lambda_i$ in Lemma 4, we acquire the equation in Theorem 2.

If $\boldsymbol{\alpha}$ is normalized as in the SRL that satisfies $\sum_{i=0}^{N-1} \alpha_i^2 = 1$, Theorem 2 is then in the form of:

$$1-h = \frac{N \sum_{i=0}^{N-1} (\alpha_i)^2 \lambda_i}{2 \sum_{j=0}^{N-1} \lambda_j}$$

□

A.3 Proof of Theorem 3

Proof. Denote filter $g(\lambda)$ as $g(\lambda) = \sum_{i=0}^K w_i (1-\lambda)^i$, $g_{even}(\lambda) = \frac{1}{2}(g(\lambda) + g(2-\lambda))$ and $g_{odd} = g(\lambda) - g_{even}(\lambda)$. The filter $g_{even}(\lambda)$ is free of odd order terms. The odd filter $g_{odd}(\lambda)$ can be seen as the gap between the full-order filter and the even-order filter.

$$\begin{aligned}
g_{even}(\lambda) &= \sum_{k=0}^{\lfloor K/2 \rfloor} w_k (1-\lambda)^{2k} \\
g_{odd}(\lambda) &= \sum_{k=0}^{\lfloor K/2 \rfloor} w_k (1-\lambda)^{2k+1}.
\end{aligned}$$

We now consider the SRL gap of the odd-order filter to illustrate the effect of removing odd-order terms. The regression problem in the spectral domain with normalized $\boldsymbol{\alpha}$ is: $\boldsymbol{\alpha} = \sigma(g(\Lambda)\boldsymbol{\beta})$,

$\sum_{i=0}^{N-1} \alpha_i^2 = 1$. Suppose $\boldsymbol{\alpha}$ and $\boldsymbol{\beta}$ is positive correlated in the form of $\mathbb{E}[\boldsymbol{\alpha}] = w\boldsymbol{\beta}, w > 0$, and $\lambda_{N-1} = 2$ for both \mathcal{G}_1 and \mathcal{G}_2 (to ensure both graphs can achieve $h = 0$).

The SRL of filter g_{odd} and g_{even} between normalized $\boldsymbol{\alpha}$ and normalized $g(\boldsymbol{\lambda})\boldsymbol{\beta}$ is:

$$\begin{aligned} L_{odd}(\mathcal{G}) &= 2 - \frac{1}{T_{odd}} \left(\sum_{i=0}^N \alpha_i^2 g(\lambda_i)_{odd} \right) \\ &= 2 - \frac{1}{T_{odd}} \left(\sum_{i=0}^{N/2} \alpha_i^2 g(\lambda_i)_{odd} + \sum_{i=N/2}^N \alpha_i^2 |g(\lambda_i)_{odd}| \right) \\ &= 2 - \frac{1}{T_{odd}} \left(\sum_{i=0}^{N/2} (\alpha_i^2 - \alpha_{N-i-1}^2) g(\lambda_i)_{odd} \right) = 2 - L_o \end{aligned} \quad (11)$$

$$L_{even}(\mathcal{G}_1) = 2 - \frac{1}{T_{even}} \left(\sum_{i=0}^{N/2} (\alpha_i^2 + \alpha_{N-i-1}^2) g(\lambda_i)_{even} \right) = 2 - L_e, \quad (12)$$

where $T_{type} = \sqrt{\sum_{i=0}^{N-1} g_{type}(\lambda_i)^2 \alpha_i^2}$.

Compare equations 11 and 12. If $g(\lambda_i)$ is of a different monotonicity against $\{\alpha_i\}$, which happens when a trained odd-filter is generalized to graphs of opposite homophily, L_o becomes negative. In contrast, L_e is always positive and benefits for reducing SRL.

Suppose L_o is the approximate SRL gap between $g(\boldsymbol{\lambda})$ and $g_{even}(\boldsymbol{\lambda})$. The instability of L_o implies $L_g(\mathcal{G}_{train}) < L_{g_{even}}(\mathcal{G}_{train})$ and $L_g(\mathcal{G}_{test}) > L_{g_{even}}(\mathcal{G}_{test})$, reflecting a larger SRL gap of full-order filters than the even-order filters.

More generally, for the cases where $\lambda_{N-1} < 2$, we can still adopt the idea of discarding odd-order terms. Rewrite $g(\boldsymbol{\lambda})$ as $g'(\boldsymbol{\lambda}) = \sum_{i=0}^K (\lambda_{mid} - \lambda)^i$, where λ_{mid} is the median of $\{\lambda_i\}$. By applying the same analysis above, we can see that it is still beneficial to remove odd-order terms from $g'(\boldsymbol{\lambda})$ to narrow the SRL gap.

□

A.4 Proof of Proposition 1

Proof. In the case where $h(\mathcal{G}_1) = 0$ and $h(\mathcal{G}_2) = 1$, denote the label difference of \mathcal{G}_1 and \mathcal{G}_2 as $\Delta \mathbf{y}_1$ and $\Delta \mathbf{y}_2$, where $\Delta \mathbf{y}_1 = (1, -1, 1, -1, \dots, 1, -1)^\top$, $\Delta \mathbf{y}_2 = (1, \dots, 1)^\top$.

Denote $U = (\mathbf{u}_0, \mathbf{u}_1, \dots, \mathbf{u}_{N-1})^\top$, where \mathbf{u}_i is the i -th eigenvector of U and $u_k(n)$ is the n -th element of \mathbf{u}_k .

On ring graphs, denote $a_{kn} = \sin(\pi(k+1)n/N)$, $b_{kn} = \cos(\pi kn/N)$, then the normalized $u_k(n)$ satisfies:

$$u_k(n) = \begin{cases} \frac{a_{kn}}{\sqrt{N/2}}, & \text{for odd } k, k < N-1 \\ \frac{b_{kn}}{\sqrt{N/2}}, & \text{for even } k \\ \frac{\cos(\pi n)}{\sqrt{N}}, & \text{for odd } k, k = N-1 \\ \frac{1}{\sqrt{N}} & \text{for even } k, k = 0 \end{cases}$$

Let the normalized spectrum of \mathcal{G}_1 be $\boldsymbol{\delta} = U^T \Delta \mathbf{y}_1 = (\delta_0, \dots, \delta_{N-1})^\top$, the normalized spectrum of \mathcal{G}_2 be $\boldsymbol{\delta}' = U^T \Delta \mathbf{y}_2 = (\delta'_0, \dots, \delta'_{N-1})^\top$.

Suppose $1 \leq i < N-1$ is odd, $\delta_i = \frac{1}{\sqrt{N/2}} \sum_{i=0}^{N-1} (-1)^i a_{ki}$, $\delta'_i = \frac{1}{\sqrt{N/2}} \sum_{i=0}^{N-1} a_{ki}$ and $\theta = \frac{\pi(i+1)}{N}$, then:

$$\begin{aligned}
\delta'_i - \delta_i &= \frac{1}{\sqrt{N/2}} \sum_{n=1}^{N/2} \sin\left(\frac{\pi(i+1)(2n-1)}{N}\right) \\
&= \frac{1}{\sqrt{N/2}} \sum_{n=1}^{N/2} \sin((2n-1)\theta) \\
&= \frac{1}{\sqrt{N/2}} \frac{\sum_{n=1}^{N/2} \sin(\theta) \sin((2n-1)\theta)}{\sin(\theta)} \\
&= \frac{1}{\sqrt{N/2}} \frac{\sum_{n=1}^{N/2} (\cos(2n-2)\theta) - \cos(2n\theta)}{2\sin(\theta)} \\
&= \frac{1}{\sqrt{N/2}} \frac{\cos(0) - \cos(N\theta)}{2\sin\theta} = 0
\end{aligned}$$

Therefore, for odd i and $1 \leq i \leq N-2$, $\delta_i = \delta'_i$. The conclusion can be generalized to even i and $1 \leq i \leq N-2$ using the same method.

For $i = 0$ and $i = N-1$, we have $\delta_0 - \delta'_0 = -\sqrt{N}$, $\delta_{N-1} - \delta'_{N-1} = -\sqrt{N}$. The spectral gap between \mathcal{G}_1 and \mathcal{G}_2 is:

$$\begin{aligned}
L_g(\mathcal{G}_1) - L_g(\mathcal{G}_2) &= \sum_{i=0}^{N-1} \frac{2(\delta_i - \delta'_i)g(\lambda_i)}{\sqrt{\sum_{j=0}^{N-1} g(\lambda_j)^2}} \\
&= \frac{2\sqrt{N}g(0) - 2\sqrt{N}g(2)}{\sqrt{\sum_{j=0}^{N-1} g(\lambda_j)^2}}
\end{aligned}$$

Therefore, the necessary condition for the spectral gap to be 0 is $g(0) = g(2)$. \square

B Dataset Details

B.1 Real-world Dataset statistics

The statistics of real-world Datasets are included in table B.1. In the node classification task, we transform heterophilic datasets into undirected ones following [9]. In the adversarial attack experiments, we select the largest connected component of each graph for attacks, training, validation and test following [38].

	Cora	Citeseer	PubMed	ACM	Chameleon	Squirrel	Cornell	Texas	Actor
Nodes	2,708	3,327	19,717	3,025	2,277	5,201	183	183	7,600
Edges	5,278	4,552	44,324	13,128	31,371	198,353	277	279	26,659
Features	1,433	3,703	500	1,870	2,325	2,089	1,703	1,703	932
Classes	7	6	3	3	5	5	5	5	5
Homophily Level	0.81	0.74	0.80	0.82	0.23	0.22	0.30	0.09	0.22

Table 5: Statistics of real-world datasets.

B.2 Synthetic Datasets.

We conduct cSBM datasets following [9] in the inductive setting. Denote a cSBM graph \mathcal{G} as $\mathcal{G} \sim \text{cSBM}(n, f, \lambda, \mu)$, where n is the number of nodes, f is the dimension of features, and λ and μ are hyperparameters respectively controlling the proportion of contributions from the graph structure and node features.

We assume the number of classes is 2, and each class is of the same size $n/2$. Each node v_i is assigned with a label $y_i \in \{-1, +1\}$ and an f -dimensional Gaussian vector $x_i = \sqrt{\frac{E}{n}}y_i u + \frac{Z_i}{\sqrt{f}}$, where $u \sim N(0, I/f)$ and Z is a random noise term.

Assume the generated graph is of average degree d , and denote the adjacency matrix as A . The graph structure of the cSBM graph is:

$$\mathbb{P}[\mathbf{A}_{ij} = 1] = \begin{cases} \frac{d+\lambda\sqrt{d}}{n} & \text{if } v_i v_j > 0 \\ \frac{d-\lambda\sqrt{d}}{n} & \text{otherwise.} \end{cases}$$

The parameter Φ discussed in the experiments is in the form of $\Phi = \arctan(\frac{\lambda}{m\mu}\sqrt{\frac{n}{f}}) * \frac{2}{\pi}$, where $m > 0$ is a constant. A larger $|\Phi|$ reflects a larger λ over μ , that is the proportion of information from the graph structure is larger.

In practice, we choose $n = 3000, f = 2000, d = 5, m = \frac{3\sqrt{3}}{2}$ for all graphs. The choices of λ and μ and the resulted homophily ratio are listed in Table B.2. As discussed in [11], only the hyperparameters μ and λ that satisfy $\lambda^2 + \frac{\mu^2 f^2}{n^2} > 1$ are guaranteed to generate informative cSBM graphs. As presented in Table B.2, all our settings satisfy the need.

Φ	+0.75	+0.50	-0.50	-0.75
λ	1.90	1.46	-1.46	-1.90
μ	0.37	0.69	0.69	0.37
Homophily Level	0.92	0.82	0.18	0.08

Table 6: Statistics of cSBM datasets.

C Experiment Details

C.1 Experimental Device

Experiments are conducted on a device with an NVIDIA TITAN V GPU (12GB memory), Intel(R) Xeon(R) Silver 4114 CPU (2.20GHz), and 1TB of RAM.

C.2 Model Architectures

For GPRGNN, GCNII, GNN_Guard and ProGNN, we rely on the official released code. For FAGCN, we implement the method with Pytorch Geometric(PyG) based on the released code. For H2GCN, we rely on the PyG version implemented by [20]. Defense models are based on the DeepRobust Library implemented versions[19]. Other methods are based on the PyG implemented versions [13]. The URL and commit number are presented in Table C.2).

	URL	Commit
GPRGNN	https://github.com/jianhao2016/GPRGNN	eb4e930
ProGNN	https://github.com/ChandlerBang/Pro-GNN	c2d970b
GNNGuard	https://github.com/mims-harvard/GNNGuard	88ab8ff
GCNII	https://github.com/chennnM/GCNII	ca91f56
FAGCN	https://github.com/bdy9527/FAGCN	23bb10f
H2GCN	https://github.com/CUAI/Non-Homophily-Large-Scale	281a1d0

Table 7: Code & commit numbers.

C.3 Hyperparameter settings

Node classification on cSBM Datasets & Common datasets For all models, we use early stopping 200 with a maximum of 1000 epochs. All hidden size of layers are set to be 64. We use the Adam optimizer and search the optimal leaning rate over $\{0.001, 0.005, 0.01, 0.05\}$ and weight decay $\{0.0, 0.0005\}$. For all models, the linear dropout is searched over $\{0.1, 0.3, 0.5, 0.7, 0.9\}$. For the model-specific hyperparameters, we refer to the optimal hyperparameters reported in corresponding papers. For MLP, we include 2 linear layers. For GCN and H2GCN, we set the number of convolutional layers be 2. For GAT, we use 8 attention heads with 8 hidden units each in the first convolutional layer, and 1 attention head and 64 hidden units in the second convolutional layer. For FAGCN, we search the number of layers over $\{2, 4, 8\}$, ϵ over $\{0.3, 0.4, 0.5\}$. For GCNII, we set $\lambda = 0.5$ and search the number of layers over $\{8, 16, 32\}$, α over $\{0.1, 0.3, 0.5\}$. For GPRGNN and EvenNet, we set the number of linear layers be 2 and $\alpha = 0.1$. For both models, we search the dropout rate for the propagation layer over $\{0.3, 0.5, 0.7\}$ and the order of graph filter over $\{4, 6, 8, 10\}$.

Against adversarial attacks. For the poisson attacks, we use a 2-layer GCN as the surrogate model. We use the strongest variant of Metattack, which is ‘‘Meta-Self’’ as the attack strategy. For the defense models, we carefully follow their provided guidelines of hyperparameter settings, and use the optimal hyperparameters as they reported. For other models, we use the Adam optimizer with leaning rate 0.01, weight decay 0.0005 and dropout rate 0.5. For FAGCN, we use 8 convolutional layers and a fixed $\epsilon = 0.3$. For GCNII, we use 16 convolutional layers and a fixed $\alpha = 0.2$. For GPRGNN and EvenNet, we set the order of graph filter be 4 in the DICE attack and 10 in poison attacks. For all models, we use early stopping 30 with a maximum of 200 epochs. Other hyperparameters are kept the same as the ones in the node-classification experiments.

C.4 Additional Defense Results

Homophily gap We include the homophily gap between training and test graph for Citeseer and ACM datasets in Fig 4 and 5. The homophily gaps of all attacks on all datasets grow larger as the perturb ratio increases.

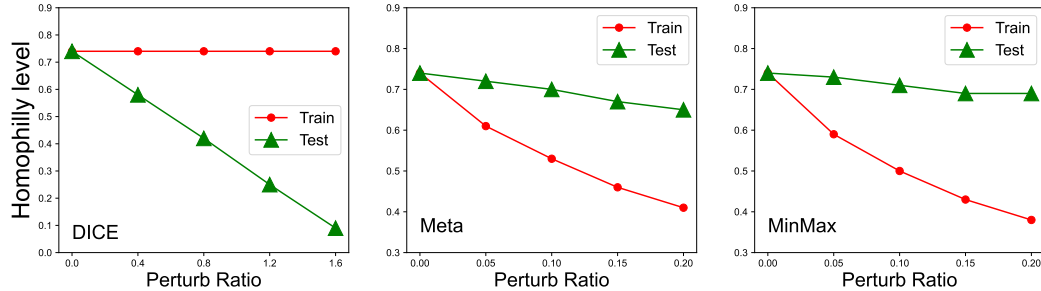


Figure 4: Homophily level of training graphs and test graphs on Citeseer after attacks.

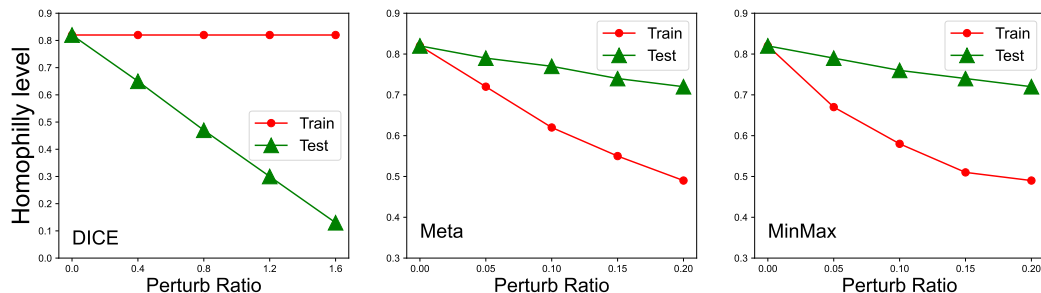


Figure 5: Homophily level of training graphs and test graphs on ACM after attacks.

Additional Experiments about Defense against Poison Attacks. Similar to DICE attacks, we provide the performance of GNN models under poison attacks of different perturb ratios. The results are presented in Figure 6 and 7. In most cases, EvenNet achieves SOTA with fewer introduced parameters.

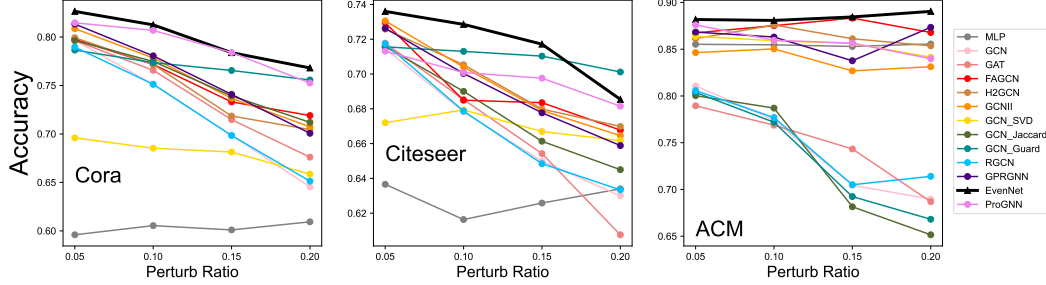


Figure 6: Meta attack on three homophilic datasets. EvenNet is marked with “ \triangle ”.

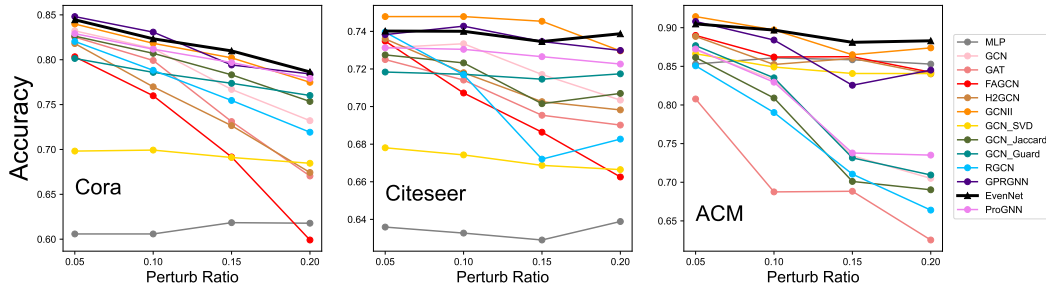


Figure 7: MinMax attack on three homophilic datasets. EvenNet is marked with “ \triangle ”.